NODULE COUNT EFFECT ON MICROSTRUCTURE AND MECHANICAL PROPERTIES OF HYPO-EUTECTIC ADI ALLOYED WITH NICKEL

**E. Colin-García [a], A. Cruz-Ramírez [a,*], J.A. Romero-Serrano [a], R.G. Sánchez-Alvarado [a],
V.H. Gutiérrez-Pérez [b], G. Reyes-Castellanos [a]**

[a] Instituto Politécnico Nacional – ESIQIE, Metallurgy and Materials Department, Mexico City, Mexico
[b] Instituto Politécnico Nacional – UPIIZ, Profesional Specific Training Department, Zacatecas, Mexico

Abstract

Samples of ductile iron alloyed with 0.88 % Ni with a nodule count of 606, 523, and 290 nod/mm² were obtained from sand cast plates of different thickness in the range from 8.46 to 25.4 mm. The effect of the nodule count was evaluated during the austempering process held at 285 °C and austempering times of 15, 30, 45, 60, 70, and 90 min. The volume fraction of high carbon austenite increased when the nodule count increased, however, the carbon content of the high carbon austenite kept almost constant. The process window was narrow, requiring a lower austempering time when the nodule count increased. The combination of a higher nodule count and low austempering temperature allowed obtaining a fine ausferritic microstructure which led to higher Brinell hardness and tensile strength. The process window was determined by XRD measurements and it was in good agreement with the microstructural and hardness evolution as the austempering time increased.

## 1. Introduction

Ductile iron (DI), also called nodular or spheroidal, has superior mechanical properties than other iron types [1]. The graphite nodules decreases the tendency of the formation of cracks and its propagation speed [2]. Austempered ductile iron or ADI is obtained by austempering and has excellent mechanical properties, such as good ductility and fracture toughness, high strength, good wear resistance, high fatigue strength, as well as rolling contact resistance and a lower density than steels [3, 4]. These properties can be achieved by a microstructure of graphite nodules in ausferrite matrix constituted by acicular ferrite (α_{ac}) and high carbon austenite (γ_{HC}) [5]. The austempering heat treatment starts with the austenitizing stage in a temperature range between 850 to 950 °C over a certain period to ensure that the matrix transforms into austenite [6]. After austenitizing, the sample is quenched to the austempering temperature in the range of 250 to 450 °C with a holding time between 0.5 and 3 hours [7]. During austempering two transformation take place, in the first stage, represented by reaction (1), the austenite unstable (γ) transform into acicular ferrite

(α_{Ac}) and high carbon austenite (γ_{HC}).

$$\gamma \rightarrow \alpha_{Ac} + \gamma_{HC} \qquad (1)$$

The second stage occurs for long austempering time, where high carbon austenite transforms into ferrite and carbides like Fe₃C or ε (both forming bainite), as it is shown in reaction (2). However, this reaction is undesirable because carbides decrease the mechanical properties due to embrittlement of the microstructure [8, 9].

$$\gamma_{HC} \rightarrow \alpha_{Ac} + Fe_3C \text{ (or } \varepsilon \text{ carbide)} \qquad (2)$$
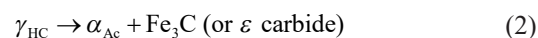
The attractive properties of ADI are related to its unique microstructure that consists of acicular ferrite and high carbon austenite referred to as ausferrite. The maximum ausferrite amount is obtained between the two transformation stages (periods), these are, the end of the first stage and the onset of the second stage, this period is referred as process window (PW), and it is represented as reaction (3) [9-11].

$$PW: \; \alpha_{Ac} + \gamma_{HC} \; \text{(stable structure)} \qquad (3)$$
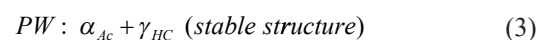
The successful production of ADI requires close control of both the foundry and heat treatment

processes. The minimum characteristics in ductile iron to obtain ADIs are [12]: a) Uniform distribution of nodule count of 100 nodule/mm^2; b) Nodularity of 85 %; c) 0.5 % maximum of carbides and non-metallic inclusions; d) 1 % maximum of porosity and micro-shrinkage, and e) Homogeneous chemical composition. Beside proper chemical compositions, suitable heat treatment parameters are also required to produce high-performance ADI. The amount and morphology of the high carbon austenite and acicular ferrite depend on the austempering parameters, temperature and holding time. At low austempering temperatures like 260 °C, ADI has very high yield strength due to the presence of fine acicular ferrite and high carbon austenite. It has been reported [13, 14] that fine ausferrite is obtained by austempering in the range of 260 – 316 °C, while coarser and feathery ausferrite is formed in the range of 316 - 450 °C. Lower austempering temperatures result in higher yield and tensile strength and hardness but with lower ductility, while, higher ductility and fracture toughness are obtained when the austempering temperature is higher than 316 °C with a corresponding decrease in the yield and tensile strength. Alloying elements are used to improve the mechanical properties or modify the austemperability of ADI. Copper, molybdenum, and nickel [8] improve the austemperability of ADI to avoid the pearlite formation during quenching while other elements such as V, Cr, B, and Mo (in excess) are avoided due to their ability to form carbides [15-18]. The effect of the casting thickness, reported as the casting modulus on the mechanical properties, was reported for a ductile iron alloyed with 0.88 wt % nickel in the as-cast condition [19]. It is well known that nodule count increases noticeably as the solidification rate increases. Nodule counts up to 2000 nod/mm^2 have been obtained on sand cast parts with thickness lower than 4 mm [20], and a highly homogeneous matrix due to the small nodule spacing [20]. The influence of nodule count on the austempering of ductile iron was also studied. M. Mourad. et al. [21] studied the effect of thin thickness on the mechanical properties of ADI austempered at 350 and 400 °C. They found that when the thickness decreased, the hardness and tensile strength increased and the highest mechanical properties were obtained to the lower austempered temperature due to a fine ausferrite microstructure. S. Chich. et al. [22] studied the effect of adding Bi on the nodule count and the fracture toughness of ADI austempered at 300 and 360 °C. The Bi addition increased the nodule count and the amount of acicular ferrite during the austempering process besides, the fracture toughness increased slightly. G. Cooper et al [23] studied the austempering kinetics for DI with different nodule counts. They found that the austempering window broadened and moved to earlier

times and that mechanical properties improved as the nodule count increased. P. Sellamutu et al [24] studied the effect of different nickel additions to ADIs austempered at different temperatures on mechanical properties and microstructure. The ADI containing 0.8 % Ni austempered at 360 °C had the higher strength and hardness. In spite of the works published on the effect of nickel on the mechanical properties of ADIs, there is little information about its effect on the processing window, microstructure, and mechanical properties of thin thickness parts during the austempering heat treatment for the process window determination. Therefore, the aim of this work is to determine the effect of the nodule count on the processing window of high nodule count ADI.

2. Experimental Procedures
2.1. Ductile iron melt

A hypo-eutectic ductile iron was produced in a 50 kg medium-frequency coreless induction furnace by using low carbon steel, pig iron, and cast iron scrap as the metallic charge. The chemical composition of the base iron was adjusted by using FeSi (75 %), high purity Ni (99 %), and high purity carbon riser. The raw materials were melted at 1450 °C, then the base iron was inoculated with 1.0 % inoculant foundry grade FeSi (75 % Si + 1 % Ca, 0.9 % Al, 1.1 % Ba) in pouring ladle and nodulized with 1.5 % of nodulizing MgFeSi (45 %Si, 8 % Mg, 3.3 % Ca, 3 % rare earths) by the sandwich technique. The cast iron was poured at 1400 °C in two green sand molds to obtain plates of (40 x 120) mm with a thickness ranging from 4.23 to 25.4 mm. The sand molds were shaken out at 30 minutes after pouring of the liquid metal into the mold. Figure 1 shows the castings produced and the plates considered for the heat treatment process.

The chemical composition was analyzed by an Oxford spark emission optic spectrograph and it was the average of five measurements. The plates of 8.46, 12.69, and 25.4 mm thickness were named DI-A, DI-B, and DI-C, respectively and were used to carry out the austempering heat treatments and the microstructural and mechanical characterization.
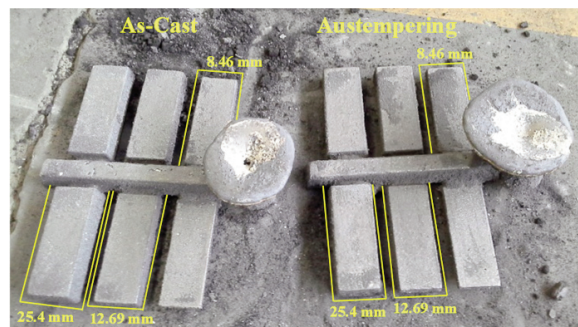

Figure 1. *Castings with plates of (40 x 120) mm with a thickness ranging from 4.23 to 25.4 mm*

2.2. Austempering heat treatment

The austempering heat treatment cycle shown in Figure 2, was carried out in two electric kilns with a heating rate of 10 °C/min. Samples of the plates of 8.46, 12.69, and 25.4 mm thickness were obtained and coated with carbon paint to avoid decarburization during the austenitizing held at 900 °C ± 5 °C with a holding time of 1 h. Then, for austempering, the samples were quickly transferred to a salt bath melt of KNO_3 and $NaNO_3$ in equal parts at 285 °C ± 5 °C. The soaking time was set at 15, 30, 45, 60, 70, and 80 min, and then water-cooled at room temperature.
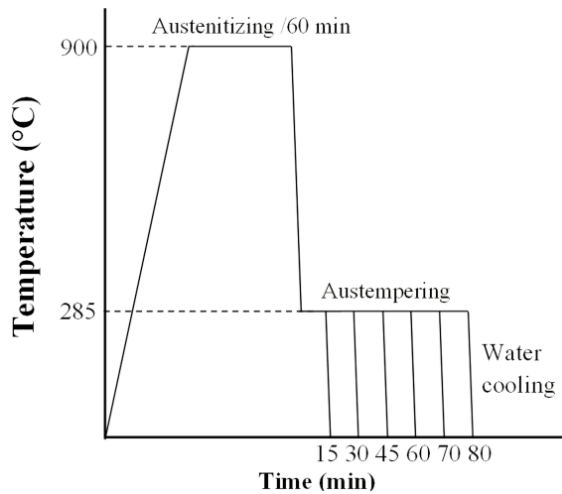

Figure 2. Austempering heat treatment scheme

2.3. Microstructural characterization

In terms of microstructural examinations, standard metallography was employed using an optical microscope Olympus PMG-3 model according to the standard ASTM A247 and the Image J software to evaluate the nodule count, average nodule size, nodularity, and the volume fraction of graphite, ferrite, and pearlite of the ductile iron in the as-cast condition. The austempered ductile iron samples were etched with nital 3 % to reveal the phases. The reported results for the optical microscopy analysis were the average of five different regions on each sample. The ADI phases and the high carbon austenite of the samples heat-treated to different time were analyzed by X-ray diffraction measurements using an X-Ray Bruker D8 Focus with monochromatic Cu $K\alpha_1$ radiation working in θ/2θ configuration. Data were collected in an angular range from 35 to 100 ° with a step size of 0.02 ° and a counting time of 2 °/min. The method reported by S. Umale et al [25] was utilized to determine the volume fraction of high carbon austenite (%Vγ_{HC}) based on equation (4) for each sample.

$$\%V\gamma_{HC} = \left[(1 + \frac{I_\alpha}{I_\gamma})R \right]^{-1} \cdot 100 \qquad (4)$$

Where: $V\gamma_{HC}$ is the high carbon austenite in volume fraction, R is a constant equal to 0.85, and I_α and $I\gamma$ are the ferrite and austenite intensities, respectively. For the %Vγ_{HC} determination, the intensity of the plane (110) was used for ferrite while the plane (111) was used for austenite [26].

The carbon content of the high carbon austenite was calculated by using equation (5) [27] for the highest retained austenite content obtained at each plate thickness.

$$\alpha_\gamma = 0.3548 + 0.0044 \, C_\gamma \qquad (5)$$

where: α_γ is the lattice parameter of austenite [nm] and C_γ is the carbon content of the high carbon austenite [wt %]. The intensities of the planes (111), (200), and (220) were considered to estimate the lattice parameter of austenite.

2.4. Mechanical properties

Samples of the austempered plates were obtained from the central region of the plates by machining in the longitudinal direction. The size and geometry of the specimens were in accordance with specifications of ASTM E8 and ASTM E10 for the tension and hardness testing, respectively. The Brinell hardness measurements were carried out using a Wilson durometer series 500. At least five measurements were taken from each sample and the average and standard deviation were reported. The tensile trials were carried out at room temperature using a universal testing machine Shimadzu with 100 kN capacity and with 5 mm/min cross-head speed. Three specimens from each plate thickness were tested for tensile trials and the average and standard deviation values were reported. For each plate thickness, only the variants with the austempering time promoting the highest retained austenite content were evaluated.

3. Results and discussion
3.1. Microstructure in the as-cast condition

The chemical composition of the ductile iron is shown in Table 1. The carbon equivalent (CE) was 4.02 which corresponded to a hypo-eutectic ductile iron. The residual Mg content was 0.06 % for an adequate nodule formation. A high silicon content was set to increase the graphitization while a low manganese content was set to avoid segregation during austempering [28]. In order to improve mechanical properties nickel was added to increase the %Vγ_{HC}, in spite of Ni delaying the stage I in austempering [29] and allowing formation a coarser acicular ferrite [30].

Table 1. *Chemical composition of ductile iron produced (wt. %)*

Heat	C	Si	Mn	P	S	Mg	Ni	Cr	Mo	Al	Cu	V	Sn	CE
DINi	3.11	2.72	0.16	0.02	0.01	0.06	0.88	0.1	<0.005	0.02	0.07	0.01	0.05	4.02

CE: Carbon equivalent. Balance Fe attached to Table 1. The three thickness evaluated were named as DI-A, DI-B, and DI-C for the thickness of 8.46, 12.69, and 25.4 mm, respectively, and Figure 3 shows the corresponding unetched and etched microstructures. The unetched microstructure showed a homogeneous distribution of spheroidal graphite for all samples with a high nodularity and nodule count. Nodule count was especially important when alloy additions were made. Low nodule counts led to the larger spacing between the graphite nodules and thus larger regions of segregation were expected while higher nodule counts broke up the segregated regions. The etched microstructure in Figure 3 revealed that the graphite nodules were contained in a pearlitic-ferritic matrix. In spite of the high cooling rates imposed in the
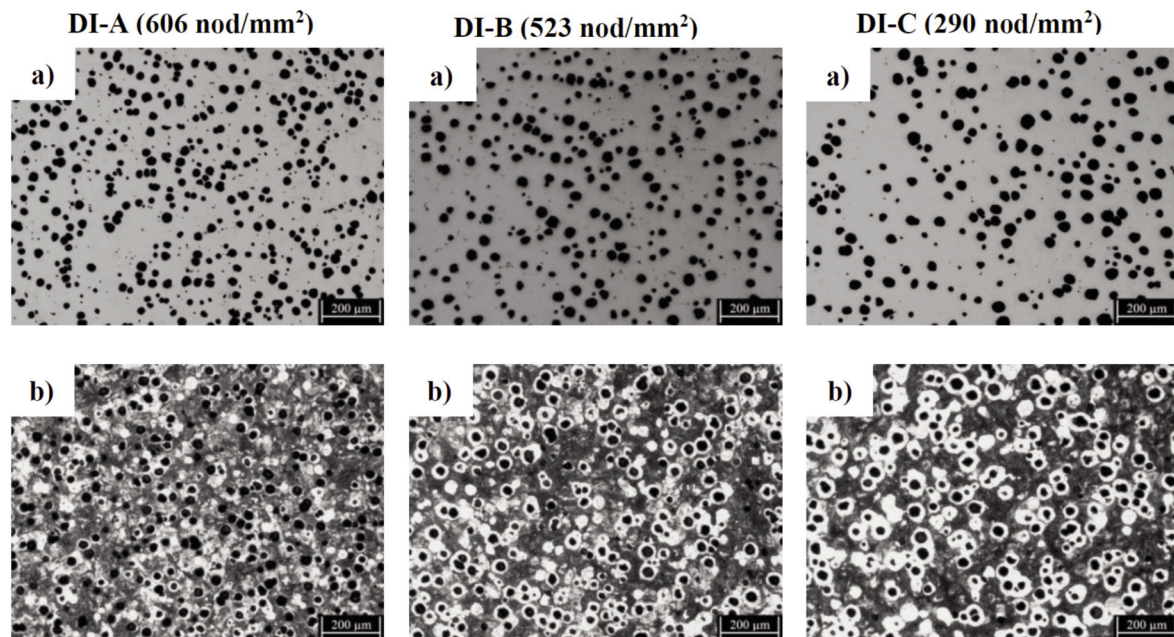
sample DI-A (8.46 mm), there was no evidence of carbides formation as cementite. The tendency to form the carbides was decreased by the addition of nickel [19]. Nickel is a good graphitiser and when added to the Fe-C system, there is a reduction of the carbon content in the eutectic, the interval between austenite-graphite and austenite-cementite eutectic transformation is increased, and the formation of carbides is suppressed [31].

Table 2 shows the nodularity, nodule count, and average nodule size values of the three thickness of the ductile iron alloyed with nickel in the as-cast condition and the volume fraction of phases formed.

The ductile iron manufactured showed a nodularity higher than 90 %, which was almost constant for the three thickness evaluated. The highest nodule count and

Table 2. *Graphite features and volume fraction of phases formed for the as-cast ductile iron*

| Sample / (thickness, mm)	Nodule count (nod/mm²)	Average nodule size (μm)	Nodularity (%)	Ferrite (%)	Pearlite (%)	Graphite (%)
DI-A (8.46)	606	28.1	90	14.5	69.5	15.98
DI-B (12.69)	523	33.4	96	28.11	59.64	12.22
DI-C (25.4)	290	42.4	91	36.52	49.63	13.83

Figure 3. *Microstructure of DI-A, DI-B, and DI-C samples for a) Unetched and b) Etched condition*

the lowest averaged nodule size were obtained for the DI-A sample which corresponded to the lowest thickness evaluated. An opposite behavior was observed for the thicker thickness. Thus, thinner section size increased the cooling rate which resulted in a high nodule count with low average nodule size. These results were in agreement with those previously reported [29, 30]. As expected, the sample DI-A with the lowest thickness showed the highest amount of pearlite and the lowest amount of ferrite while the sample DI-C showed the opposite behavior. The sample DI-B presented a volume fraction of phases between samples DI-A and DI-C. The ferrite phase showed an increase when the thickness was increased while pearlite formation was enhanced by high cooling rate solidification achieved when the casting thickness decreased.

3.2. Microstructure in the Austempered condition

Figure 4 shows the microstructures of Ni alloyed ADI with different austempering times for the three thickness evaluated.

The austempering temperature was set to obtain a microstructure of fine ausferrite. The microstructures in Figure 4 show a mixture of dark needles constituted by fine acicular ferrite and high carbon austenite which was observed as little white blocks. The evolution of the sample ADI-C showed that at an austempering time of 15 min, the microstructure was composed mainly of martensite. When the time increased to 30 min, the microstructure contained a mixture of ausferrite and martensite. At a longer austempering
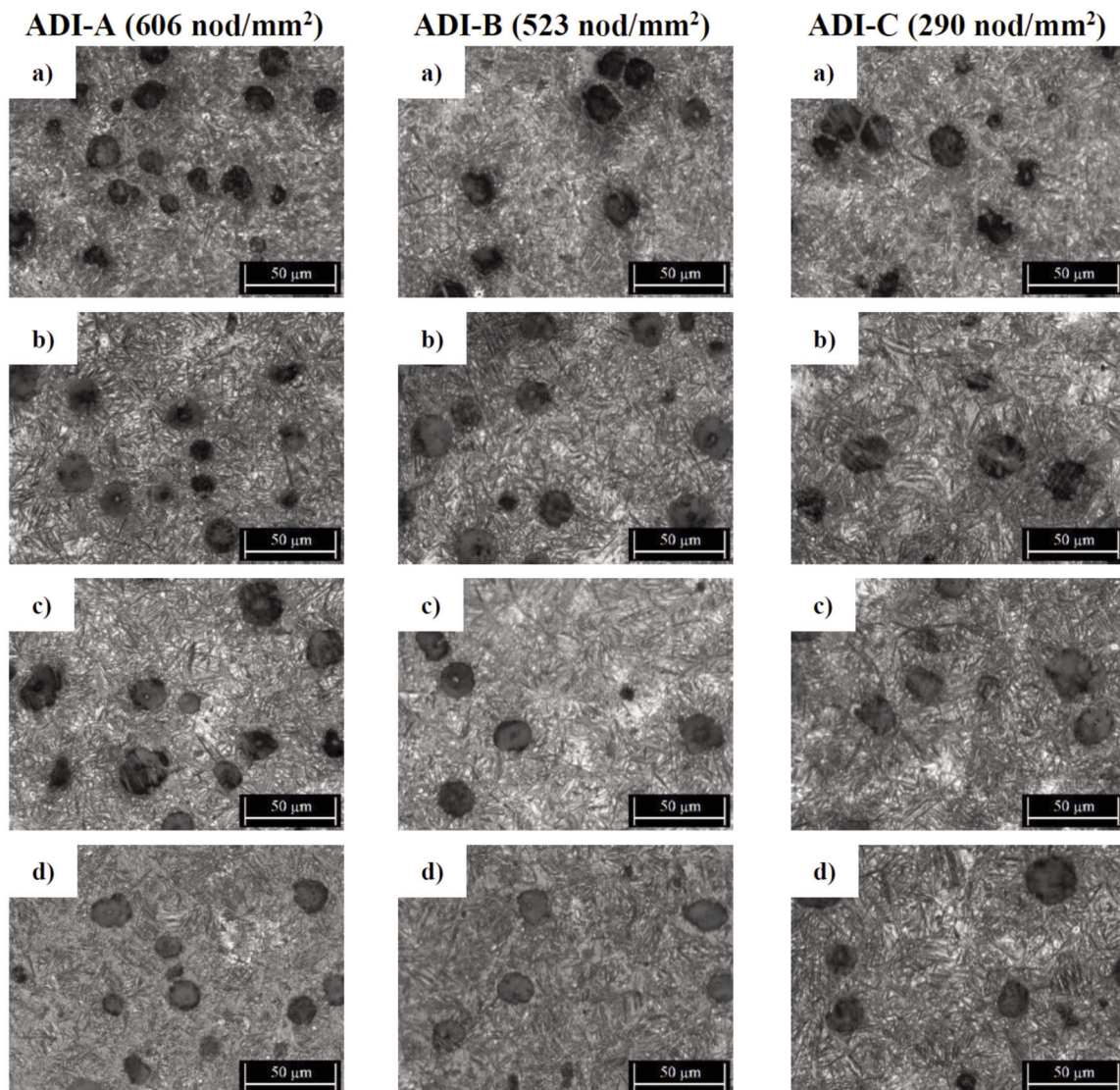
Figure 4. *Microstructural evolution of ADI alloyed with Ni after austenitizing at 900 °C for 60 min and austempering at 285 °C for various times a) 15 min, b) 30 min, c) 45 min, d) 60 min, and on next page e) 70 min, and f) 80 min*
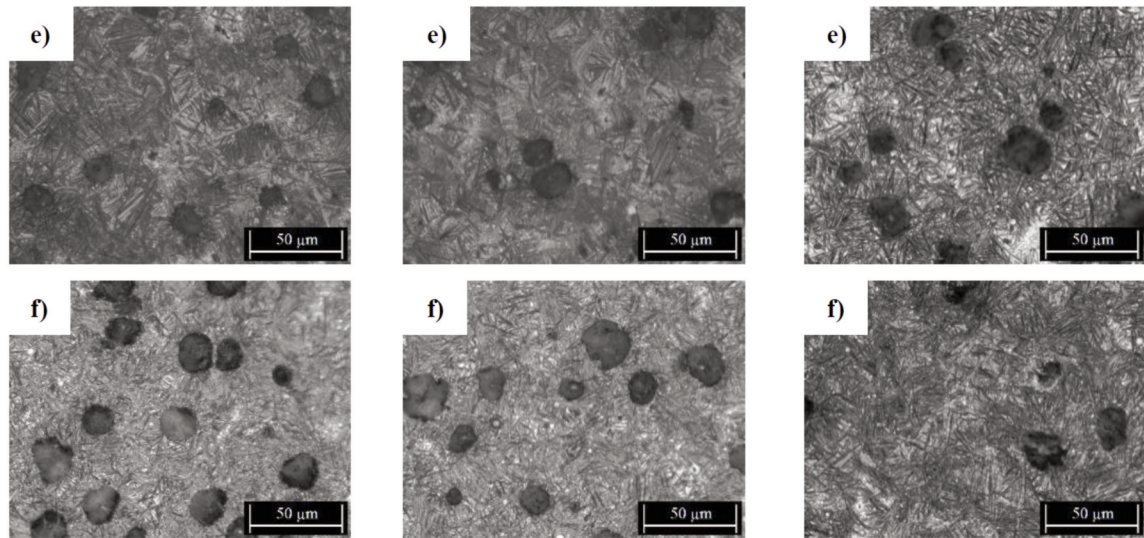
***Figure 4.** Microstructural evolution of ADI alloyed with Ni after austenitizing at 900 °C for 60 min and austempering at 285 °C for various times e) 70 min, and f) 80 min*

time of 45 min and 60 min, the microstructure consisted mainly of ausferrite with little martensite. At a still longer austempering time of 70 min, the microstructure was fully ausferritic consisting of a mixture of acicular ferrite and a high amount of carbon enriched austenite (γ_{HC}). At the longest austempering time of 80 min, the microstructure consisted of ferrite plus precipitated carbides (bainite). The results in Figure 4 show the microstructural evolution during the austempering process where the process window (PW) occurred. The sample ADI-C showed that the end of the first stage of the PW presented at the austempering time of 70 min while the second stage of the PW started at 80 min, therefore, the austempering time of 70 min represented a fully ausferritic microstructure. When the nodule count increased, like in samples ADI-B and ADI-A, the microstructural evolution was similar, however, the boundary of the PW decreased to lower times. For the samples ADI-B and ADI-A, the PW was set at 45 and 30 min, respectively. Therefore, when the nodule count increased, the PW took place at a shorter time, this behavior matched with the results reported by E. Chiniforush et al [32]. The high nodule count contributed to the improvement of the ausferritic microstructure [21], as shown in Figure 4, where the

microstructure of ADI-A was finer than in the ADI-B and ADI-C samples. In addition, the high nodularity obtained for the three thickness evaluated shown in Figure 3 and reported in Table 2 increased the high carbon austenite volume fraction [33]. The XRD patterns of the samples austempered at different times are shown in Figure 5 for the three thickness evaluated. The volume fraction of high carbon austenite (%Vγ_{HC}) was determined based on the procedure reported by S. Umale et al [25].

Table 3 shows the results of the XRD analysis and the application of equation (4) to determine the influence of the austempering time on the high carbon austenite.

It is observed from Table 3 that the %Vγ_{HC} increased first, reached a maximum value and then decreased. The highest value of γ_{HC} (11.51 vol. %) for ADI-A which contained the highest nodule count (606 nod/mm^2) was higher than the highest value of γ_{HC} (10.04 vol. %) corresponding to ADI-C with the lowest nodule count (290 nod/mm^2). The ADI-B sample showed intermediate values between ADI-A and ADI-C samples. Thereby, when the nodule count increased, the amount of nodule-matrix interface areas also increased, the distance between nodules

***Table 3.** Volume fraction of high carbon austenite to different austempering times*

Sample/	%Vγ_{HC}					
(Nodule count, nod/mm^2)	Austempering time (min)					
	15	30	45	60	70	80
ADI-A (606)	11.18	**11.51**	11.13	10.55	9.86	8.38
ADI-B (523)	9.72	10.03	**10.98**	10.59	9.84	9.21
ADI-C (290)	7.45	7.93	9.25	9.95	**10.04**	9.85

decreased and then the carbon diffusion was favored obtaining an increase in the amount of high carbon austenite [34]. The %Vγ_{HC} in all cases was small and this occurred because at low austempering

temperatures the mainly micro-constituent in ausferrite matrix was ferrite. During the austempering heat treatment the ferrite was formed from the unstable austenite by nucleation and growth in the solid-state process, however at lower temperatures such as 285 °C, the supercooling was very high and consequently, the nucleation rate was greater, thus more ferrite was nucleated a low temperature [35]. The low amount of %Vγ_{HC} in ADIs was due to the diffusion of a low amount of carbon atoms when the transformation occurred at low austempering temperatures then the ferrite formed rejects the carbon atoms surrounding it but at this temperature, the diffusion was slow [36]. Similar results were reported by P. Sellamuthu et al [24] with values of 12, 17, and 21 for the %Vγ_{HC} in ADI alloyed with 0.8 %Ni and austempered at 320, 340, and 360 °C, respectively.

Figure 6 shows the effect of the austempering time on the high carbon austenite formation for the three thicknesses of the ADI alloyed with nickel.

Considering that the PW was a period that comprised two stages during the austempering process where a maximum value of γ_{HC} was reached and then a decrease occurred as austempering time proceeded then, the PW should be located in the range of two austempering times. The bars located at the bottom of the graph in Figure 6 represent the PW for each thickness of the ADI evaluated which contained a different nodule count. It was observed for ADI-A which contained the highest nodule count that the PW occurred in the range of time between 15 and 45 min, reaching the highest %Vγ_{HC} at 30 min. Otherwise, for the ADI-C with the lowest nodule count, the PW occurred in the range from 60 to 80 min with the highest %Vγ_{HC} located at 70 min. Therefore, as the nodule count increased, the PW occurred at lower austempering times, this behavior matched with the results reported by E. Fras et al [37] where a high
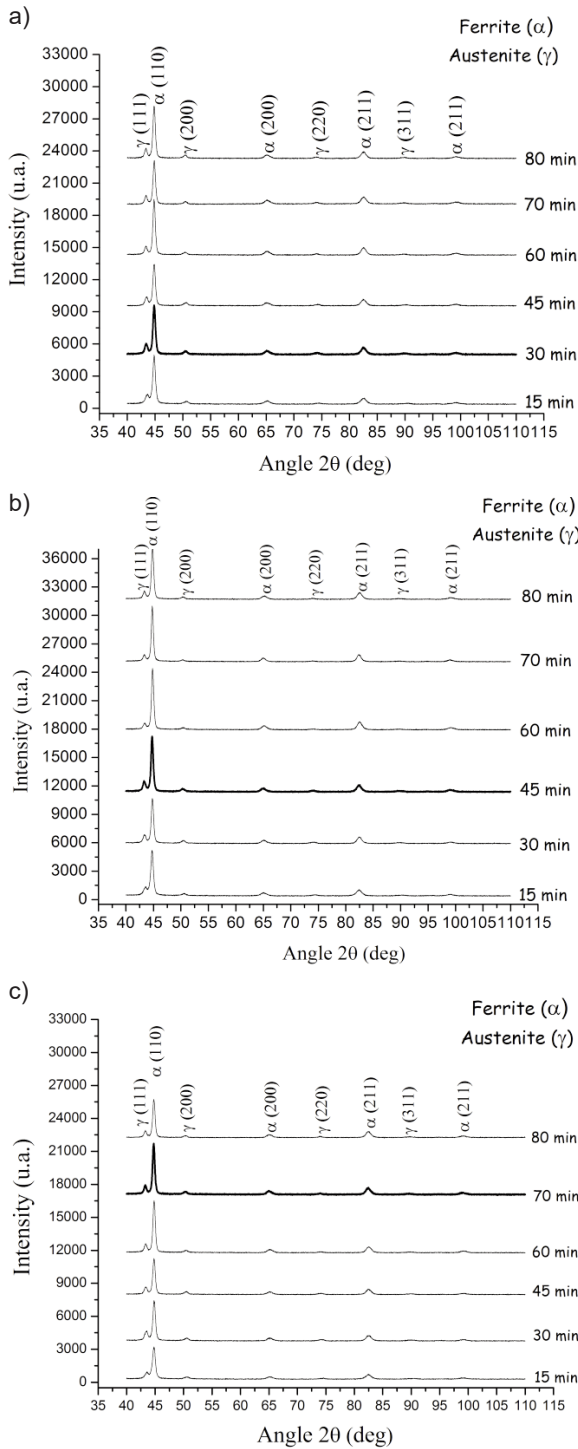
Figure 5. XRD patterns at different austempering times for the three thickness samples a) ADI-A, b) ADI-B, and c) ADI-C
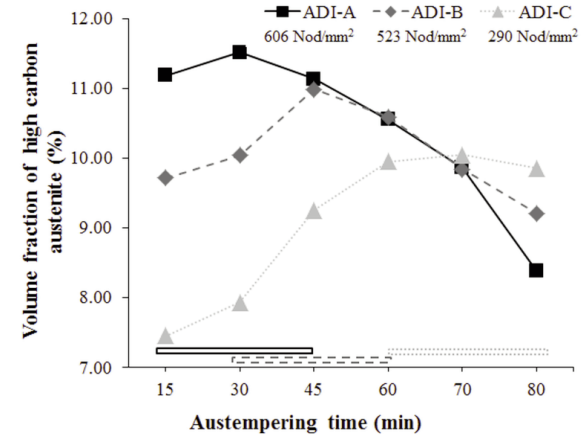

Figure 6. Effect of the austempering time on the high carbon austenite

nodule count decreased the diffusional lengths for carbon, reducing the austempering time.

The carbon content of the high carbon austenite (C_γ) is shown in Table 4 for the highest retained austenite content obtained at each plate thickness. The results of C_γ obtained for the three ADI samples were very similar, therefore, there was no relationship between the nodule count with C_γ. J. Yang et al. [38] pointed out that the C_γ related to the austempering temperature, when the austempering temperature increased, the C_γ increased too. The results of C_γ obtained matched with those reported by A. Sosa et al. [34] where values of 1.545 and 1.568 of C_γ were determined for 265 and 1200 nod/mm², respectively for ADI austempered at 280 °C.

Table 4. *The carbon content of the high carbon austenite for the highest retained austenite contents*

Sample/ (Nodule count, nod/mm²)	% V γ_{HC}	C_γ
ADI-A (606)	11.51	1.739
ADI-B (523)	10.98	1.753
ADI-C (290)	10.04	1.751

3.3. Mechanical Properties

Table 5 shows the effect of the austempering time on the Brinell hardness for the ADI samples with different nodule count and represent the average of five hardness measurements.

It was observed that the hardness values of the ADI's were higher than for the DI in the as-cast condition. High hardness values were reported for lower austempering times, then a decrease occurred, followed by a hardness increase as the austempering time proceeded. The lowest hardness value for each ADI sample corresponded to the austempering time at which the highest value of high carbon austenite was obtained. The hardness was directly related to the microstructural evolution reported in Figure 4. The ADI-A sample showed a high hardness value of 426.32 HBW to the austempering time of 15 min

which was attributed to a high amount of martensite. When the austempering time reached 30 min, the hardness decreased to 396.32 HBW due to the microstructure which was mainly ausferrite and after reaching 45 min, the hardness increased to 403.28 HBW with a slight trend to increase as austempering time increased, this behavior was due to the decomposition of high carbon austenite into ferrite and carbides. The PW can be determined considering the austempering time which comprised the minimum hardness value situated in the middle of two values with higher hardness [36]. The other two ADIs samples showed the same behavior as ADI-A, except that the minimum hardness value was obtained for higher austempering times. This means that, if the nodule count decreased, a higher austempering time was required to reach the PW. Therefore, the evolution of hardness matched with the high carbon austenite results in the PW determination.

The PW was also observed in Figure 7 where the bars located at the bottom of the graph represented the PW for each ADI variant evaluated, as was reported by P. Parhad et al [36]. It was observed that the highest hardness values were obtained for the ADI-A sample which contained the highest nodule count and hardness decreased as the nodule count decreased.

P. Sellamuthu et al [24] reported Brinell hardness values of 266, 266, and 268 HBW for an ADI alloyed
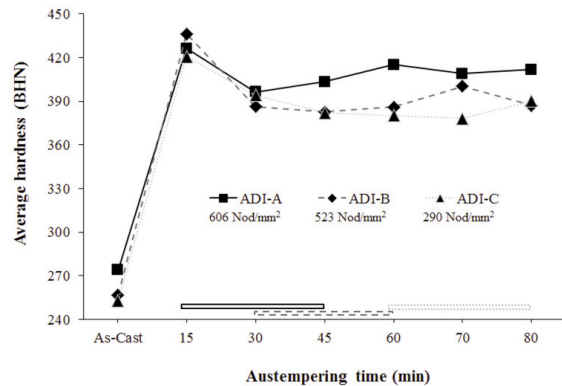
Figure 7. *Austempering time influence on Brinell hardness average*

Table 5. *Brinell hardness as a function of the austempering time*

| Sample/ (Nodule count, nod/mm²)	Hardness (HBW)						
	Austempering time (min)						
	As-Cast	15	30	45	60	70	80
ADI-A (606)	274.26 ± 2.6	426.32 ± 3.6	**396.32** ± 2.5	403.28 ± 2.3	415.15 ± 2.4	409.04 ± 2.6	411.82 ± 2.1
ADI-B (523)	257.38 ± 3.3	436.43 ± 1.3	386.43 ± 2.4	**382.71** ± 2.1	385.97 ± 2.4	400.33 ± 2.8	387.17 ± 2.9
ADI-C (290)	253.13 ± 3.8	420.74 ± 1.5	394.09 ± 2.4	382.27 ± 2.6	380.97 ± 2.5	**378.23** ± 2.9	390.28 ± 3.8

with 0.8 % Ni and austempered at 320, 340, and 360 °C, respectively. The hardness values reported in Table 5 were considerably higher than those obtained for P. Sellamuthu et al [24] because of the high refinement of the ADI microstructure constituted by a finer ferrite and austenite obtained by lower austempering temperature and a high nodule count.

For each plate thickness, only the variants with the austempering time promoting the highest retained austenite content were evaluated. The tensile strength was evaluated for the samples with the highest %Vγ$_{HC}$ for each plate thickness. Therefore, the samples with austempering times 30, 45, and 70 min for ADI-A, ADI-B, and ADI-C, respectively were evaluated. Table 6 shows the tensile properties and standard deviation results.

Table 6. *Tensile properties as a function of the austempering time*

Sample/ (Nodule count, nod/mm²)	ADI-A (606)	ADI-B (523)	ADI-C (290)
Austempering time (min)	30	45	70
Tensile strength (MPa)	815.56 ± 5.3	810.06 ± 4.8	776.21 ± 5.9
Yield strength (MPa)	607.49 ± 4.8	582.36 ± 4.1	513.92 ± 4.9
Elongation (%)	1.43 ± 0.19	1.12 ± 0.08	0.89 ± 0.09

The effect of the nodule count on the tensile properties reported in Table 6 and Figure 8, show that increasing the nodule count, the average tensile and yield strengths increased, reaching a maximum value of 815 and 607 MPa, respectively for ADI-A (606 nod/mm²). When the nodule count decreased to 290 nod/mm², the tensile and yield strengths were reduced to 776 and 513MPa, respectively. It has been reported [21] that an increase in the nodule count, increased the mechanical properties in ADI. In addition, an ADI
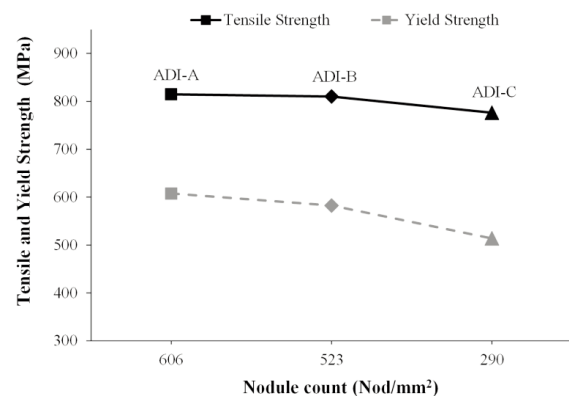
Figure 8. *Nodule count effect on tensile and yield strength*

alloyed with 0.8 % Ni austempered at 320 °C showed a tensile and yield strength of 815 and 630 MPa, respectively [24] which was in agreement with the results reported in Figure 8. Table 6 shows that elongation was slightly increased when the nodule count increased, however, the elongation values were low due to the low austempering temperature used to increase the strength of cast iron. Nevertheless, a similar elongation trend for ADI with different nodule count was reported by G. Cooper [23].

4. Conclusions

The effect of the nodule count was evaluated for a 0.88 %Ni ADI of different thickness austempered at 285 °C and different austempering times. The results obtained are summarized as follows:

1. The sand cast model with plates of 8.46, 12.69, and 25.4 mm promoted nodule counts of 606, 523, and 290 nod/mm², respectively.

2. The volume fraction of high carbon austenite (%Vγ$_{HC}$) increased with the nodule count, reaching a maximum value of 11.51 %.

3. The austempering time required to obtain the highest %Vγ$_{HC}$ was shorter for high nodule count, because the carbon diffusion was increased by a decrease in the distance between nodules. However, the nodule count variation did not have an effect on the carbon content of the high carbon austenite.

4. The Brinell hardness, tensile strength, and elongation also increased with the nodule count due to a finer ausferrite.

5. The evolution of hardness matched the high carbon austenite results in the PW determination.

Acknowledgments

References

[1] T. J. Marrow, H. Centinel, M. Al-Zalmah, S. Macdonald, P. J. Withers, J. Walton, Fatigue Fract. Engng. Mater. Struct, 23 (5) (2002) 425–434.

[2] M. A. Neri, C. Carreño, Mater. Charact., 51 (4) (2003) 219–224.

[3] S. K. Putatunda, S. Kesani, R. Tackett, G. Lawes, Mat. Sci. Eng. A, 435-436 (2006) 112-122.

[4] B. Stokes, N. Gao, P. A. S. Reed, Mat. Sci. Eng. A, 445–446 (2007) 374–385.

[5] J. M. Han, Q. Zou, G. C. Barber, T. Nasir, D. O. Northwood, X. C. Sun, P. Seaton, Wear, 290–291 (2012) 99–105.

[6] K. M. Kumar, P. Hariharan, P. Venkateshwaran, S.

Tamilarasan, Trans. Indian Inst. Met., 68 (2015) S67–S71.

[7] L. Meier, M. Hofmann, P. Saal, W. Volk, H. Hoffmann, Mater. Charact., 85 (2013) 124–133.

[8] O. Eric, M. Jovanovic, L. Sidjanin, D. Rajnovic, J. Min. Metall. Sect. B-Metall., 40 (1) B (2004) 11–19.

[9] H. R. Erfian-Naziftoosi, N. Haghdadi, A. R. Kiani-Rashid, J. Mater. Eng. Perform., 21 (8) (2012) 1785–1792.

[10] A. Gazda, J. Therm. Anal. Calorim., 102 (2010) 923–930.

[11] O. Erick, T. Brdaric, N. Stojsavljevic, M. Tonic, N. Grahovac, R. Đuricic, Metall. Mater. Eng., 16 (2) (2010) 91-102.

[12] J. R. Keough, K. L. Hayrynen, G. L. Pioszak, AFS proceedings, 10-129 (2010) 1-15.

[13] S. Panneerselvam, C. J. Martis, S. K. Putatunda, J. M. Boileau, Mater. Sci. Eng. A, 626 (2015) 237–246.

[14] G. Wenbang, C. Guodong, L. Li, H. Jing, Z. Zhonghe, China Foundry, 9 (2) (2012) 143–147.

[15] Ch. F. Han, Y. F. Sun, Y. Wu, Y. H. Ma, Metallogr. Microstruct. Anal., 4 (2015) 135–145.

[16] S. Laino, J. A. Sikora, R. C. Dommarco, Wear, 265 (2008) 1–7.

[17] P. Yun-cheng, J. Hui-Jin, L. jin-Hai, L. Gou-Lu, Mater. Sci. Eng. A, 529 (2011) 321–325.

[18] Ch. F. Han, Q. Q. Wang, Y. F. Sun, J. Li, Metallogr. Microstruct. Anal., 4 (2015) 298–304.

[19] E. Colin-García, A. Cruz-Ramírez, G. Reyes-Castellanos, J. A. Romero-Serrano, R. G. Sánchez-Alvarado, M. Hernández-Chávez, J. Min. Metall. Sect. B-Metall., 55 (2) B (2019) 283–293.

[20] E. Fras, M. Górny, Arch. Foundry Eng., 9 (3) (2009) 45–48.

[21] M. M. Mourad, K. M. Ibrahim, M. M. Ibrahim, A. A. Nofal, 68th WFC, February 7-10, Chennai, India, 2008, p. 161–166.

[22] L. Shen-Chih, H. Cheng-Hsun, C. Chao-Chia, F. Hui-Ping, Metall. Mater. Trans. A, 29 A (1998) 2511–2521.

[23] G. Cooper, A. Roebuck, H. Bayati, R. Elliott, Int. J. Cast Met. Res., 11 (2009) 227–235.

[24] P. Sellamuthu, D. G. Harris-Samuel, D. Dinakaran, V. P. Premkumar, L. Zushu, S. Seetharaman, CMSME 2018 IOP conf Series: Mater. Sci. Eng., Febrary 24-26, Bangkok, Thailand, 2018, p. 1–7.

[25] S. Umale, A. Likhite, D. R. Peshwe, S. U. Pathak, Indian Foundry J., 60 (9) (2014) 28–36.

[26] H. Bakhshinezhad, A. Honarbakhshraouf, H. Abdollah-Pour, Phys. Met. Metallogr., 120 (2019) 441-446.

[27] C. S. Roberts, J. Metal., 5 (1953) 203-204.

[28] S. Dhanasekaran, A. Vadiraj, G. Balachandran, M. Kamaraj, Trans. Indian Inst. Met., 63 (2010) 779–785.

[29] O. Erić, D. Rajnović, S. Zec, L. Sidjanin, M. T. Jovanović, Mater. Charact., 57 (4–5) (2006) 211–217.

[30] U. Batra, S. Ray, S. R. Prabhakar, J. Mater. Eng. Perform., 13 (1) (2004) 64–68.

[31] I. Minkoff, Alloy Cast Iron Systems, The Physical Metallurgy Of Cast Iron, John Wiley and Sons Ltd., Norwich, England, 1983, p. 185-188.

[32] E. Akbarzadeh-Chiniforush, N. Iranipour, S. Yazdani, China Foundry, 13 (3) (2016) 217–222.

[33] A. A. Nofal, M. Ramadan, R. Adbel-Karim, Proceedings of the 2002 World Conference of ADI AFS Publication, September 26-27, Louisville, Kentucky USA, 2002, p. 15-28.

[34] A. D. Sosa, M. D. Echeverría, O. J. Moncada, N. Míngolo, J. A. Sikora, J. Mater. Process. Technol., 209 (2009) 5545–5551.

[35] S. K. Putatunda, P. K. Gadicherla, J. Mater. Eng. Perform., 9 (2) (2000) 193–203.

[36] P. Parhad, S. Umale, A. Likhite, J. Bhatt, Trans. Indian Inst. Met., 65 (2012) 449–458.

[37] E. Fraś, M. Górny, E. Tyrała, H. Lopez, Mater. Sci. Tech, 28 (12) (2012) 1391–1396.

[38] J. Yang, S. K. Putatunda, Mat. Sci. Eng. A, 406 (2005) 217-228.

UTICAJ BROJA NODULA NA MIKROSTRUKTURU I MEHANIČKE OSOBINE KOD HIPOEUTEKTIČNOG AUSTEMPEROVANOG NODULARNOG LIVA LEGIRANOG NIKLOM

E. Colin-García [a], A. Cruz-Ramírez [a,*], J.A. Romero-Serrano [a], R.G. Sánchez-Alvarado [a], V.H. Gutiérrez-Pérez [b], G. Reyes-Castellanos [a]

[a] Nacionalni politehnički institut – ESIKIE, Odeljenje za metalurgiju i materijale, Meksiko Siti, Meksiko
[b] Nacionalni politehnički institut – KUPIIZ, Odeljenje za stručno usavršavanje, Zacatecas, Meksiko

Apstrakt

Uzorci nodularnog liva legiranog sa 0,88% Ni, gde broj nodula iznosi 606, 523 i 290 nod/mm2, dobijeni su iz kalupa od peska različite debljine u rasponu od 8,46 do 25,4 mm. Uticaj broja nodula je ispitan tokom postupka austemperovanja na 285 °C nakon 15, 30, 45, 60, 70 i 90 min. Zapreminski udeo austenita se povećao kada se povećao broj nodula, međutim sadržaj ugljenika u austenitu je ostao konstantan. Granica specifikacije je bila ograničena, što je zahtevalo da se skrati vreme postupka austemperovanja kada se broj nodula povećao. Kombinacija većeg broja nodula i niže temperature tokom termičkog postupka omogućila je dobijanje fine ausferitne mikrostrukture što je dovelo do veće tvrdoće po Brinelu i zatezne čvrstoće. Granica specifikacije je određena pomoću XRD merenja i bila je u skladu sa nastankom mikrostrukture i tvrdoćom kako se vreme termičkog postupka povećavalo.

Ključne reči: Nodularni liv; Broj nodula; Austemperovani nodularni liv; Granica specifikacije; Nikl